HIBONITE-SPINEL INCLUSIONS FROM THE ALH A77307 CO3.0 CHONDRITE: A FIB/TEM APPROACH. Jangmi Han[1] and Adrian J. Brearley[1], [1]Department of Earth and Planetary Sciences, MSC03-2040, 1 University of New Mexico, Albuquerque, NM 87131, USA (E-mail: jmhan@unm.edu; brearley@unm.edu).

Introduction: Thermodynamic equilibrium condensation calculations for a gas of solar composition have predicted hibonite to be one of the earliest-formed refractory phases, second only after corundum [e.g., 1]. Although comparatively rare relative to other refractory phases found in CAIs, hibonite has been found in CAIs from several different groups of carbonaceous chondrites [2]. Hibonite shows a variety of trace element patterns and is a carrier of isotopic anomalies (e.g., ^{26}Al) [2,3]. Therefore, hibonite has considerable potential to reveal conditions and processes in the very early stages of the formation of the solar system.

In this study, we describe the microstructure and textural relationships of refractory constituent phases in hibonite-spinel inclusions, one of the dominant types of CAI found in CO3 chondrites [4], by utilizing FIB techniques combined with TEM. The goal of this study is to provide additional constraints on the formational processes and conditions of hibonite-spinel inclusions.

Methods: We investigated in detail individual hibonite-spinel inclusions from a thin section of the ALH A77307 CO3.0 chondrite using elemental X-ray mapping and BSE imaging on a FEI Quanta 3D FEG-SEM/FIB. FIB techniques were used to prepare a TEM section from one hibonite-spinel inclusion (CAI 03). The FIB section was extracted and characterized in detail using a variety of TEM techniques, including bright-field TEM, dark-field scanning TEM, electron diffraction, and EDS X-ray analysis using a JEOL 2010 high resolution TEM and a JEOL 2010F FASTEM FEG scanning TEM.

Results: In this study, we have found 10 hibonite-spinel inclusions among a total of 84 CAIs from the one thin section of ALH A77307. These hibonite-spinel inclusions (10-70 μm in size) usually consist of randomly-oriented, lath-shaped hibonite grains embedded in spinel, consistent with the observations of [4]. Hibonite ranges in length from 12 μm to 40 μm and in width from 2.5 μm to 20 μm. Fine-grained, subrounded to elongated perovskite is a common accessory phase with a size range of 0.2-5.5 μm. Perovskite is typically enclosed by spinel, but is also sometimes present included within hibonite. Melilite is an extremely rare phase and was found in only one of the 10 inclusions. Melilite is irregular in shape and ~10 μm across.

We selected one inclusion (CAI 03) for further microstructural characterization by TEM. As shown in Fugure 1, CAI 03 is an irregularly-shaped inclusion (70 μm x 40 μm in size) and has typical characteristics of this type of CAI.

The FIB section from CAI 03 was cut across several hibonite grains (Fig. 1). The FIB section consists of spinel and hibonite with minor perovskite and melilite. Hibonite grains are typically lath-shaped and parallel to subparallel with each other. Hibonite grains show various thicknesses and lengths; 0.2-5 μm long and 60 nm-2.5 μm wide. Individual hibonite grains are elongated parallel to the *c* axis. Two perovskite grains 1-2 μm in size were found; one is a subrounded grain enclosed by hibonite and the other is an elongated grain in contact with hibonite and spinel. Although SEM BSE imaging indicates that the region where the FIB section was prepared does not contain melilite, minor melilite is present interstitially between the hibonite laths and is usually elongated, 0.2-2 μm long. Spinel grains are usually irregular in shape and range in size from 0.5 μm to 3.5 μm. Pores occur throughout the FIB section with elongated shapes and lengths of 0.2-3.5 μm.

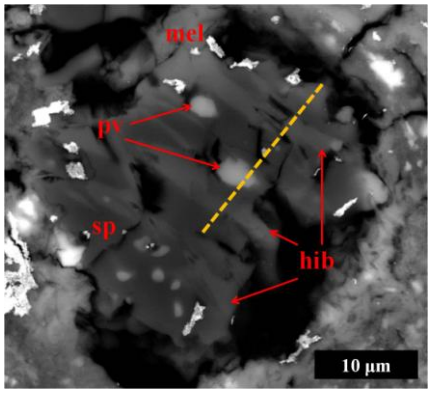

Figure 1. SEM BSE image of hibonite-spinel inclusion (CAI 03) from ALH A77307. The dotted line indicates the location of the FIB section examined in this study. hib: hibonite, pv: perovskite, sp: spinel, and mel: melilite.

An important TEM observation from CAI 03 is that there is a crystallographic orientation relationship between hibonite and spinel. Electron diffraction analysis shows that individual hibonite and spinel grains are randomly oriented. However, analysis of Fast Fourier Transform patterns obtained from high-resolution TEM images of hibonite and spinel from two different parts of the FIB section show that the two phases can have a crystallographic orientation relationship. This relationship is the same for both occurrences with the [010] zone axis of hibonite parallel to the [011] zone axis of spinel and the (001) plane of hibonite parallel to the (111) plane of spinel, i.e., $[010]_{hibonite}$ // $[011]_{spinel}$ and $(001)_{hibonite}$ // $(111)_{spinel}$. No crystallographic orientation relationships between hibonite and perovskite have been

observed.

Analytical electron microscopy shows that hibonite in the FIB section shows some variation in composition with 0.5-2.2 wt.% SiO_2, 0.85-7.7 wt.% TiO_2, 0.3-4.6 wt.% MgO, and low concentrations (<0.5 wt.%) of V_2O_3, Cr_2O_3, and FeO. These compositional variations are found between and within single hibonite grains, but we did not find zoning in individual hibonite grains or any systematic change within the FIB section. On a plot of Σ(Mg+Fe+Si+Ti) cations vs. Al cations per 19 O anions, hibonite compositions from the FIB section lie close to or on a 1:1 line implying the coupled substitutions of $Mg^{2+} + Ti^{4+} \leftrightarrow 2Al^{3+}$ and $Mg^{2+} + Si^{4+} \leftrightarrow 2Al^{3+}$. A plot of Σ(Mg + Fe) cations against Σ(Ti + Si) cations per 19 O anions in hibonite shows that all the TEM EDS analyses fall below a 1:1 correlation line, indicating that some Ti is present as Ti^{3+} which directly substitutes for Al^{3+}. However, this conclusion may not be robust, because we assumed that all Ti is present as Ti^{4+} when quantifying the TEM EDS data. Further analysis is necessary to confirm this possible substitution.

Spinel is very close to $MgAl_2O_4$ with <0.6 wt.% FeO. Perovskite is nearly pure $CaTiO_3$ with <0.4 wt.% FeO and <0.6 wt.% V_2O_3. Regardless of whether perovskite is surrounded by hibonite, perovskite has a uniform composition. Melilite is very close to gehlenite with an åkermanite content up to 3.8 mol.% (<0.6 wt.% MgO).

Discussion: Based on our SEM and TEM observations, hibonite appears to be the first phase to form in individual hibonite-spinel inclusions including CAI 03, followed by perovskite, melilite, spinel, and diopside. This inferred formation sequence of minerals is generally consistent with the predicted sequence from thermodynamic equilibrium condensation calculations [1]. The irregular shapes and porous textures of these CAIs also support a condensation origin. It is therefore very likely that the random orientation of hibonite laths in individual inclusions is the result of high-temperature condensation of individual hibonite laths from a nebular gas, followed by random accumulation into aggregates.

Some perovskite grains in hibonite-spinel inclusions from ALH A77307 are enclosed by hibonite whereas most are embedded within spinel. Previous studies of hibonite-bearing inclusions from other carbonaceous chondrites have also commonly reported that perovskite occurs included in hibonite laths [e.g., 5]. These observations suggest that some perovskite might form before hibonite. We attribute the inclusion of perovskite within hibonite to a continuum of hibonite condensation over a limited temperature range where perovskite is also a stable condensate from the nebular gas [1,6]. Condensing hibonite crystals could trap early-condensing perovskite grains and would overgrow them as hibonite continued to condense. As nebular cooling proceeded, hibonite condensation would eventually cease, but perovskite kept condensing and was later enclosed by spinel once spinel condensation commenced at lower temperatures.

Based on textural relations, in CAI 03 the majority of melilite appears to have formed at a late stage in the condensation sequence, contrary to thermodynamic equilibrium condensation calculations which predict that melilite condenses before spinel [1,7]. Instead, the presence of spinel in crystallographic continuity with hibonite demonstrates that melilite condensation was inhibited and that spinel condensed directly onto hibonite. An explanation for this behavior may be provided by a consideration of the crystallographic orientation relationship between spinel and hibonite. The (111) plane of spinel consists of a hexagonal-close-packed array of oxygen ions with Al in octahedral sites, which resembles the (001) plane of hexagonal-structured hibonite. These structural similarities favor epitaxial nucleation and growth of spinel on hibonite surfaces. If the activation energy for epitaxial nucleation of spinel on hibonite was lower than for nucleation of melilite, then spinel condensation may have been kinetically more favorable. Under these conditions, the depletion of Al in the gas phase may have inhibited melilite condensation, resulting in melilite-poor or melilite-free hibonite-spinel inclusions. Similarly, [7] concluded that the morphology of spinel in two hibonite-spinel inclusions from the Murchison CM2 chondrite was directly inherited from hibonite during gas-solid condensation, based on SEM observations from platy crystals in these inclusions composed of hibonite at one end close to the core of the inclusions and spinel on the opposite end near their outer rim.

Conclusions: Our SEM and TEM observations indicate that hibonite-spinel inclusions in ALH A77307 formed by high-temperature gas-solid condensation from the cooling solar nebula. The crystallographic orientation relationship between hibonite and spinel provides evidence of epitaxial nucleation and growth of spinel, which may have lowered the activation energy for spinel nucleation compared with that of melilite. As a consequence, melilite condensation was inhibited, resulting in a rarity of melilite in this type of CAI in CO3 chondrites.

Acknowledgements: This research was funded by NASA Cosmochemistry grant NNX11AK51G to A. J. Brearley (PI).

References: [1] Ebel D. S. (2005) *MESS II*, p.253-277. [2] MacPherson G. J. (2003) *In Treatise on Geochemistry*, p.201-246. [3] Ireland T. R. (1990) *GCA 54*, 3219-3237. [4] Russell S. S. et al. (1998) *GCA, 62*, 689-714. [5] Krot A. N. et al. (2004) *MAPS 39*, 1517-1553. [6] Yoneda S. and Grossman L. (1995) *GCA 59*, 3413-3444. [7] MacPherson G. J. et al. (1984) *Proc. 15th Lunar Planet. Sci. Conf.*, C299-C312.